Kusumah, Ferdi Perdana; Vuorsalo, Simo; Kyyrä, Jorma

A direct three-phase to single-phase AC/AC converter for contactless electric vehicle charger

Published in:
17th European Conference on Power Electronics and Applications (EPE'15 ECCE-Europe), Geneva, 8-10 September 2015

DOI:
10.1109/EPE.2015.7309422

Published: 01/01/2015

Document Version
Peer-reviewed accepted author manuscript, also known as Final accepted manuscript or Post-print

Please cite the original version:
Kusumah, F. P., Vuorsalo, S., & Kyyrä, J. (2015). A direct three-phase to single-phase AC/AC converter for contactless electric vehicle charger. In *17th European Conference on Power Electronics and Applications (EPE'15 ECCE-Europe), Geneva, 8-10 September 2015* (pp. 1-10). IEEE.
https://doi.org/10.1109/EPE.2015.7309422

A Direct Three-Phase to Single-Phase AC/AC Converter for Contactless Electric Vehicle Charger

Ferdi Perdana Kusumah, Simo Vuorsalo, and Jorma Kyyrä
Department of Electrical Engineering and Automation
School of Electrical Engineering
AALTO UNIVERSITY
P.O. Box 13000
FI-00076 Aalto, Finland
E-mail: ferdi.kusumah@aalto.fi
URL: http://eea.aalto.fi/en/

Keywords

<<AC/AC converter>>, <<Battery charger>>, <<Contactless power supply>>, <<Electric vehicle>>, <<Resonant converter>>, <<Soft switching>>.

Abstract

This paper proposes an attractive direct line-frequency three-phase to a higher frequency single-phase AC/AC converter for a contactless electric vehicle charger. It removes a DC-link capacitor of a conventional AC/AC converter but has a smaller number of bi-directional switches than a matrix converter. It operates using injection and free-oscillation modes based on a zero-current switching mechanism. Circuit descriptions including a topology, commutations and a modulation strategy are discussed using some illustrations and diagrams. An on-off control is used to simplify control of resonant current. Simulation results to study some effects due to different coupling factor and load are then presented to show converter's performance and capabilities in contactless power transfer.

Introduction

Reliability and ease of maintenance of a power transfer device can be improved by integrating a Contactless Power Transfer (CPT) module in it. By eliminating a physical conductor, the module reduces a risk of electric shock, eliminates sparking and increases mobility of a power receiver device [1][2]. A typical CPT electric vehicle (EV) charger system is illustrated in Figure 1. It usually consists of a primary coil driven by a resonant inverter to produce an alternating-current (AC) waveform. If an AC source is used, then an AC to direct-current (DC) converter in the primary rectifier is needed as an intermediate stage. The stage requires a DC-link capacitor C_{DC} which can be bulky and expensive. The primary circuit will supply current to a secondary circuit through an inductive coupling mechanism and rectify it to charge an EV's battery. In industrial environments, only a three-phase AC source is commonly used. Therefore, the converter is recommended to produce the AC waveform in the coil directly from its AC source to remove the C_{DC} capacitor which can lead to reduced system size and cost [3][4][2].

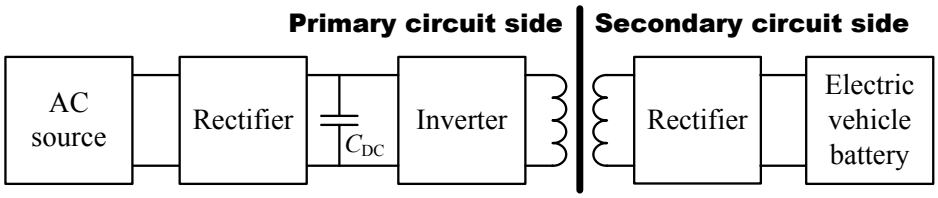

Figure 1: A typical CPT system.

The authors of [5] proposed a three-phase to single-phase matrix converter driving a resonant circuit for a CPT application. It manages to exclude the DC-link capacitor but uses six bi-directional switches and a hard-switching principle in its operation that can increase its cost and decrease its lifetime. Another form

of a direct AC/AC converter was proposed in [2], where a reduced amount of bi-directional switches is used. A free-oscillation mode was introduced to decrease its switching frequency. However, the single-phase to single-phase converter suffers an output current amplitude drop at each zero crossing of its input voltage that can reduce its average transferred power.

This paper therefore proposes a three-phase to single-phase direct AC/AC converter that has a fewer number of bi-directional switches compared to the matrix converter while eliminates a zero crossing current drop in [2]. Its output current is controlled by a simple on-off controller and a zero-current switching (ZCS) principle is used to minimize switching losses. A resonant frequency of around 80 kHz is chosen to increase its output power capacity and reduce the size of circuit inductors [6]. Detailed analysis of secondary pick-up circuit and bi-directional power transfer mechanism will not be discussed in this paper.

This paper is organized as follows. In Circuit Description, the converter topology and its basic working principles are introduced. A modulation and control schemes will also be explained in the same section. Steady-State Analysis describes on how to simplify the secondary circuit and calculate a steady-state behavior of the system, so each component's characteristic can be studied. Simulation Results section describes some important waveforms of the circuit under no-load and load conditions. Lastly, conclusions of the paper are drawn.

Circuit Description

Circuit topology

A circuit diagram of the proposed converter is given in Figure 2. The primary side consists of a three-phase source connected to a series-resonant circuit (L_p and C_p) through three bi-directional input switches Sa, Sb and Sc. The switch symbol all over this paper are represented by an ideal insulated-gate bipolar transistor (IGBT) with anti-parallel diode. The switches will create AC current with a higher frequency than the input to transfer power to a secondary pick-up. The transfer involves an inductive coupling mechanism on a loosely-coupled air-core transformer (L_p and L_s). One extra pair of bi-directional switches Sd is connected in-parallel with the resonant circuit and needed to perform free-oscillation current commutations. The secondary circuit will rectify AC waveform and use it to charge an EV's battery $v_o(t)$.

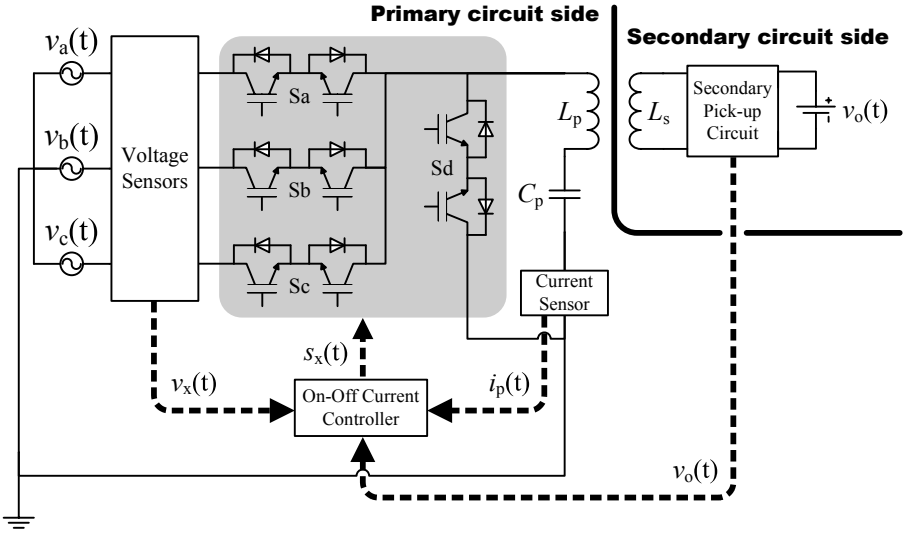

Figure 2: A proposed direct AC/AC converter topology. Dashed arrows of $v_x(t)$, $v_o(t)$ and $i_p(t)$ represent measured signals while $s_x(t)$ indicates a control signal.

The on-off current controller takes input voltage measurements $v_x(t)$ and resonant current information $i_p(t)$, as well as secondary circuit output voltage $v_o(t)$ to determine a correct switching frequency. The controller will maintain the resonant current amplitude to match a suitable reference point derived from $v_o(t)$ through a control signal $s_x(t)$. Since the primary and secondary sides are coupled, controlled primary resonant current leads to controlled secondary (output) current. This paper only focuses on the primary circuit side, so the current reference value is assumed to be known.

Circuit commutation

Figure 3 shows illustrations of possible injection and free-oscillation current commutation cases of the primary circuit. In those cases, only one input phase is used to illustrate them, but the same principles can

be applied to the other phases. In the first case (Figure 3a), the controller is made to supply the resonant circuit by selecting the maximum of voltage absolute values among the three-phase inputs which can be defined as:

$$\mathrm{Max}(v) = \mathrm{Max}(|v_{\mathrm{a}}(\mathrm{t})|, |v_{\mathrm{b}}(\mathrm{t})|, |v_{\mathrm{c}}(\mathrm{t})|). \tag{1}$$

The Max(v) symbol will be used throughout this paper to represent the operation. In Figure 3a, it is assumed that the appropriate value comes from $v_{\mathrm{a}}(\mathrm{t})$ at its positive voltage cycle. The conducting switch and diode are marked with bold lines. The current is flowing from the input to the resonant circuit since the input is in a positive cycle. This direction is regarded as a positive direction as marked beside the inductor current $i_{\mathrm{p}}(\mathrm{t})$ and with a bold arrow in the figure.

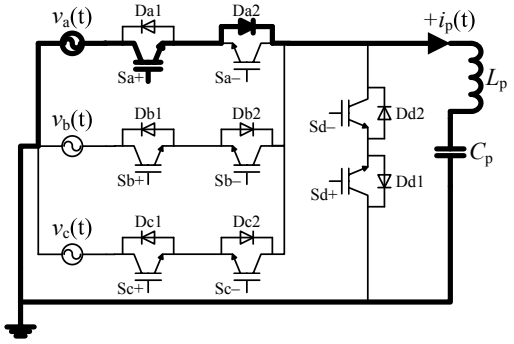

(a) Case 1: Sa+ and Da2 are conducting.

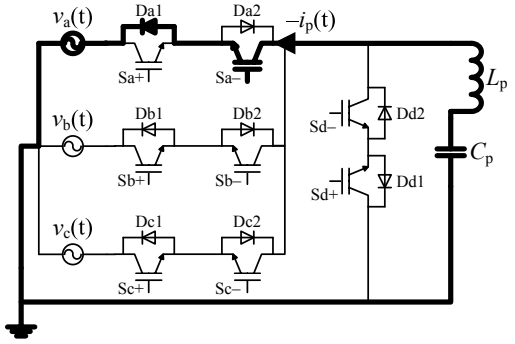

(b) Case 2: Sa− and Da1 are conducting.

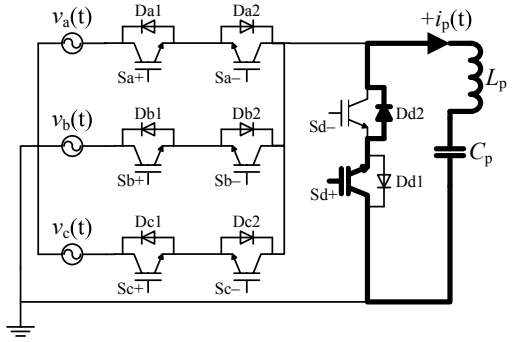

(c) Case 3: Sd+ and Dd2 are conducting.

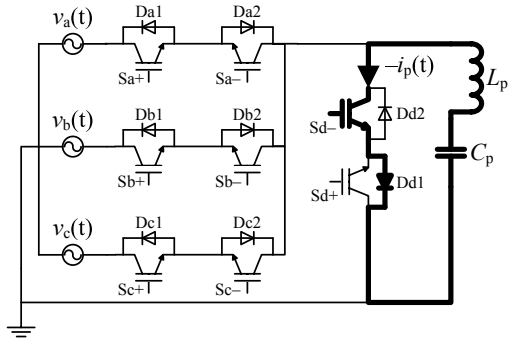

(d) Case 4: Sd− and Dd1 are conducting.

Figure 3: Commutation possibilities of the proposed AC/AC converter from a primary circuit point of view. Bold lines indicate current flow.

Figure 3b describes a case of input current flow during a negative cycle of the input voltage. The current is flowing in the opposite direction (negative) of the first case. Case 1 and 2 are considered as an injection mode. The two cases are used to pump the resonant current to a desired level. The injection principles are still valid if the input is taken either from $v_{\mathrm{b}}(\mathrm{t})$ or $v_{\mathrm{c}}(\mathrm{t})$. In either situation, the operational components will be Sb and Db pair for $v_{\mathrm{b}}(\mathrm{t})$ or Sc and Dc pair for $v_{\mathrm{c}}(\mathrm{t})$.

The last two cases (3 & 4) are considered as a free-oscillation mode. The input is not used and only one pair of bi-directional switches (Sd+ and Sd−) is used. In this case, the switches are utilized based on the resonant current flow direction, therefore at a pure free-oscillation mode, the switching frequency of either Sd+ or Sd− is equal to the resonant frequency. Other method of switching will be to turn on both Sd at the same time to reduce the frequency, but this case will not be discussed in this paper. The free-oscillation mode is used to reduce the amplitude of the resonant current by letting it decays through a circuit load or a resistance. In an ideal case without a resistive load, the mode will cause the current to circulate indefinitely. By using injection and free-oscillation modes, the current amplitude can be made to follow a certain reference value. Complete switching case possibilities of the converter are given in Table I.

A commutation waveforms illustration within one cycle of an input phase is presented in Figure 4. Each input is indicated by $v_{\mathrm{a}}(\mathrm{t})$, $v_{\mathrm{b}}(\mathrm{t})$ and $v_{\mathrm{c}}(\mathrm{t})$ while a gate signal of each switch is expressed by $s_{\mathrm{xy}}(\mathrm{t})$ where the subscript x represents each input and y marks a current direction (i.e. $s_{\mathrm{a+}}(\mathrm{t})$ is a gate signal for Sa+ switch). It can be seen that all switches are turned-on and off during zero crossings of primary resonant current $i_{\mathrm{p}}(\mathrm{t})$. Sa+, Sb+ and Sc+ are switched at the positive cycle of the input phases. The switches as well as Sd+ are only conducting positive primary current. On the contrary, Sa−, Sb− and Sc−

Table I: Switching cases of the proposed direct AC/AC converter

Case	Input source	Input cycle	Turned-on switch	Turned-on diode	Current direction
1	$v_{\mathrm{a}}(\mathrm{t})$	+	Sa+	Da2	+
2	$v_{\mathrm{a}}(\mathrm{t})$	−	Sa−	Da1	−
3	0	not available	Sd+	Dd2	+
4	0	not available	Sd−	Dd1	−
5	$v_{\mathrm{b}}(\mathrm{t})$	+	Sb+	Db2	+
6	$v_{\mathrm{b}}(\mathrm{t})$	−	Sb−	Db1	−
7	$v_{\mathrm{c}}(\mathrm{t})$	+	Sc+	Dc2	+
8	$v_{\mathrm{c}}(\mathrm{t})$	−	Sc−	Dc1	−

are switched on the negative cycle of the input, and together with Sd−, only passing negative primary current. The switching actions will produce discrete voltage at the input of the resonant circuit and this voltage is marked by a bold line in the first plot and indicated by $v_{\mathrm{res}}(\mathrm{t})$. During Max($v$) periods, the number of non-zero $v_{\mathrm{res}}(\mathrm{t})$ depends on the number of related zero crossing transitions as indicated by vertical dashed arrows in the $i_{\mathrm{p}}(\mathrm{t})$ plot. As a result of ZCS, a turn-off delay effect may occur when a zero crossing transition happens near the border of Max(v) as highlighted in Figure 4. The turn-off delay time is marked by t_{del}. The free-oscillation commutation period is expressed by t_{free}. The total duration of t_{free} within one period of the input phase depends on a required resonant current amplitude, therefore the higher the amplitude demand, the shorter the total duration of t_{free} within that time span. It can also be seen that the on duration of any pulse is equal to a half of the resonant frequency's period.

Converter modulation scheme

Block diagram and flowchart of the system are presented in Figure 5. They have been applied at a simulation level. From the block diagram side, zero crossings of resonant current are used to construct gate signals for Sa+, Sb+ and Sc+ (rise crossing) as well as Sa−, Sb− and Sc− (fall crossing). The crossing signal will only be produced if the reference current amplitude is greater than the actual one. The reference value is derived from the secondary circuit output voltage. The signal construction from the zero crossings is only used for injection gate signals. The voltage selector block will calculate Max(v) of a three-phase input taken from voltage sensors which will be used in injection mode. On the other hand, free-oscillation mode signals are built using sign information of the current to drive Sd+ and Sd−.

The main issue with the signal generation approach is a need of a starting pulse to trigger the primary current. Therefore, before all operations in every block take place, a trigger signal is used. The initiation process is described by gray blocks in Figure 5b. In the beginning, the controller will first check whether there is an ongoing current i_{p} in the primary circuit. If there is none, then a rectangular pulse (created using rise and fall step functions) will be used to draw current from an appropriate input phase to excite the resonant circuit until a first current zero crossing occurs. The controller will then proceed to its normal operation by checking whether the current peak value i_{peak} is smaller than a reference value I_{ref}. If it is true, then the injection will take place and the resonant peak-to-peak current will increase. If the condition is false, then all converter switches will be turned-off except the Sd pair to activate the free-oscillation mode.

Detailed operations inside some blocks in Figure 5a are given in Figure 6. The zero crossing detector block separates and selects rise and fall crossing signals $i_{\mathrm{zc}}(\mathrm{t})$ into $zc_{\mathrm{rise}}(\mathrm{t})$ and $zc_{\mathrm{fall}}(\mathrm{t})$. The selection is performed on a condition $i_{\mathrm{peak}}(\mathrm{t}) < I_{\mathrm{ref}}$. It also produces unselected version of both signals which are $zc_{\mathrm{rise}}(\mathrm{t})_{\mathrm{clock}}$ and $zc_{\mathrm{fall}}(\mathrm{t})_{\mathrm{clock}}$. A voltage selector block will select the appropriate input signal based on (1). In positive and negative injection modes, it is assumed that $v_{\mathrm{a}}(\mathrm{t})$ is the selected input voltage. Positive injection happens when the voltage is in a positive cycle ($\mathrm{Sgn}(\mathrm{Max}(v)) = +$). A $s_{\mathrm{a+}}(\mathrm{t})$ gate signal will then be produced using $zc_{\mathrm{rise}}(\mathrm{t})$ and $zc_{\mathrm{fall}}(\mathrm{t})_{\mathrm{clock}}$. In the negative injection case, $zc_{\mathrm{fall}}(\mathrm{t})$ and $zc_{\mathrm{rise}}(\mathrm{t})_{\mathrm{clock}}$ will be used instead to produce $s_{\mathrm{a-}}(\mathrm{t})$. The gate signals are produced inside the Max(v) region of the chosen input. The same injection principles can be applied if the chosen input phase is either $v_{\mathrm{b}}(\mathrm{t})$ or $v_{\mathrm{c}}(\mathrm{t})$. The turn-off delay effect introduced in Figure 4 is also shown in Figure 6. In either case, the corresponding active switch will be Sb or Sc pair respectively. In free-oscillation, the gate signal is achieved through a multiplication between either *pos* and *sigma* (for Sd+) or *neg* and *sigma* (for Sd−). $v_{\mathrm{res}}(\mathrm{t})$ is the produced discrete voltage injecting the resonant circuit (not shown in Figure 6).

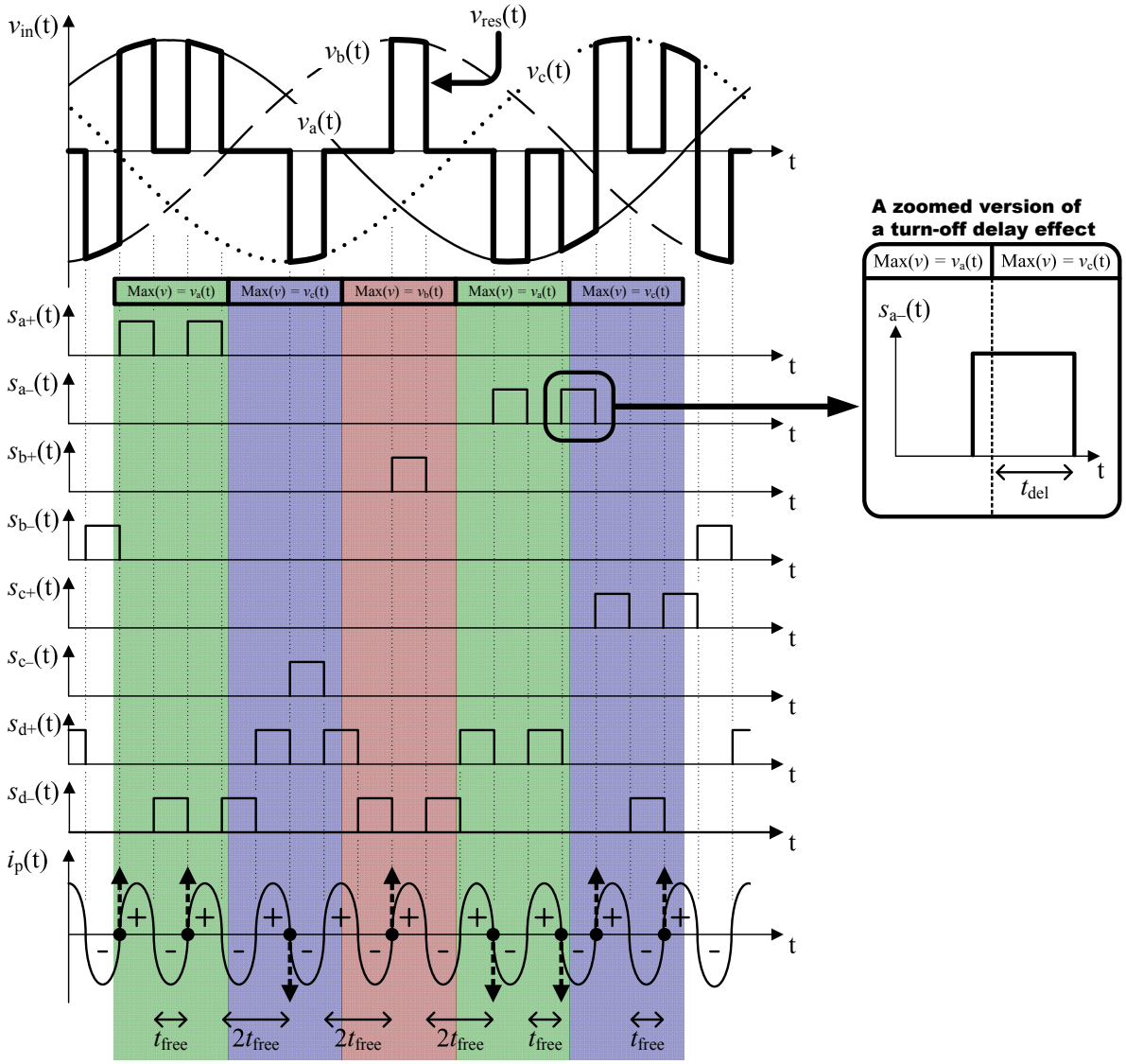

Figure 4: Converter commutation waveforms.

Steady-State Analysis

Fundamental harmonic analysis will be used to further analyze the primary and secondary circuits due to a fact that the resonant network has a higher harmonic voltages filtering effect [7]. Therefore, the input square wave source can be approximated by its fundamental sinusoidal waveform. The analysis will focus on steady-state behaviors of the circuits.

To simplify the modeling process, some assumptions must be made, which are, the three-phase input is balanced with a constant amplitude, all electrical components are ideal, the line frequency is constant, and the battery is behaving as a resistor. Since the converter utilizes three input phases one at a time during its commutations, an equivalent circuit of it with a single phase source can be used to model the system as given in Figure 7a. The C_s value is assumed to be infinite. According to [7], the rectifier, together with the load capacitor and resistor on the secondary circuit can be approximated by $R_{eq} = 8R_L/\pi^2$ through a power transfer analysis. This can lead to a further simplification given in Figure 7b. Using a phasor domain analysis, a set of circuit equations can be obtained, which is:

$$\begin{cases} V_s \angle \phi = \frac{\mathbf{i_p}}{j\omega C_p} + \mathbf{i_p} j\omega L_p - \mathbf{i_s} j\omega M \\ 0 = \mathbf{i_s} R_{eq} + \mathbf{i_s} j\omega L_s - \mathbf{i_p} j\omega M \\ M = k\sqrt{L_p L_s}, \end{cases} \tag{2}$$

V_s value can be obtained by assuming the switching frequency is very large compared to the line frequency. V_s is then an amplitude of a fundamental component of a square signal $v_{avg}(t)$ given in Figure 8.

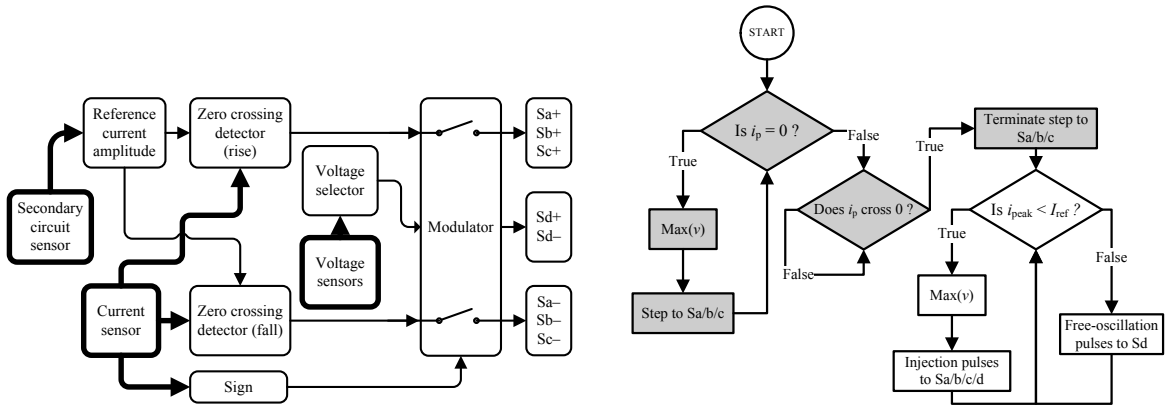

(a) A primary circuit block diagram. (b) A primary circuit flowchart.

Figure 5: Primary circuit general descriptions.

The plot is basically the same as the first one in Figure 4, but the switching frequency is much higher than a line frequency in this case. The amplitude of $v_{\mathrm{avg}}(\mathrm{t})$ can be approximated as follows:

$$V_{\mathrm{A}} = V_{\max}\frac{\sum_{k=0}^{k=\mathrm{Round}(N)}\sin(2\pi f_l(t_{\mathrm{i}}+k\frac{T_{\mathrm{s}}}{2}))}{\mathrm{Round}(N)}, \quad k=2n+1, \quad n=0,1,2,\ldots, \tag{3}$$

where $V_{\max}$ is the amplitude of the line voltage which equals to $\sqrt{2}V_{\mathrm{rms}}$. The equation is achieved by rectangular approximation and averaging each switched voltage element from t_{i} to t_{f} (half period of $v_{\mathrm{avg}}(\mathrm{t})$). Since N can be in a decimal form, a round operation is needed for the summation. A simpler calculation method is also exist to calculate V_{A}, by assuming $v_{\mathrm{res}}(\mathrm{t})$ covers half of the area between t_{i} and t_{f} of the input (Figure 8). Amplitude V_{A} can then be obtained by calculating an average value integral of the corresponding phase from t_{i} to t_{f} and dividing the result by 2. With this approach, the amplitude is $V_{\mathrm{A}} = 3V_{\max}/(2\pi)$. Through a Fourier analysis, fundamental component amplitude of $v_{\mathrm{avg}}(\mathrm{t})$ is equal to:

$$V_{\mathrm{s}} = 4V_{\mathrm{A}}/\pi. \tag{4}$$

The equations in (2) can be combined by eliminating $\mathbf{i_s}$, and this leads to:

$$V_{\mathrm{s}}\angle\phi = \frac{\mathbf{i}_{\mathrm{p}}}{\mathrm{j}\omega C_{\mathrm{p}}} + \mathbf{i_p}\mathrm{j}\omega L_{\mathrm{p}} + \frac{\mathbf{i_p}\omega^2 M^2}{R_{\mathrm{eq}}+\mathrm{j}\omega L_{\mathrm{s}}}. \tag{5}$$

By multiplying the last term in (5) with its complex conjugate, the equation can be split into its real and imaginary parts, which has a form of:

$$\frac{\mathbf{i_p}\omega^2 M^2}{R_{\mathrm{eq}}+\mathrm{j}\omega L_{\mathrm{s}}} = \frac{\mathbf{i_p}\omega^2 M^2 R_{\mathrm{eq}}}{{R_{\mathrm{eq}}}^2+\omega^2{L_{\mathrm{s}}}^2} - \frac{\mathbf{i_p}\mathrm{j}\omega^3 M^2 L_{\mathrm{s}}}{{R_{\mathrm{eq}}}^2+\omega^2{L_{\mathrm{s}}}^2}. \tag{6}$$

Resonant frequency

Since the converter operates at its resonant frequency, the frequency is needed to analyze current and voltage across its components. To find the frequency, all reactive components in (5) and (6) must be set to zero as presented below:

$$0 = \frac{1}{\mathrm{j}\omega_0 C_{\mathrm{p}}} + \mathrm{j}\omega_0 L_{\mathrm{p}} - \frac{\mathrm{j}\omega_0^3 M^2 L_{\mathrm{s}}}{{R_{\mathrm{eq}}}^2+\omega_0^2{L_{\mathrm{s}}}^2} \tag{7}$$

$$({L_{\mathrm{s}}}^2 L_{\mathrm{p}} C_{\mathrm{p}} - M^2 L_{\mathrm{s}} C_{\mathrm{p}})\omega_0^4 + ({R_{\mathrm{eq}}}^2 L_{\mathrm{p}} C_{\mathrm{p}} - {L_{\mathrm{s}}}^2)\omega_0^2 - {R_{\mathrm{eq}}}^2 = 0. \tag{8}$$

The last equation is in a biquadratic form and can be solved by substitution. It says that there are four resonant frequencies available which are:

$$\omega_{0_{1,2}} = \pm\sqrt{\frac{-frac+\sqrt{frac^2+4\frac{{R_{\mathrm{eq}}}^2}{den}}}{2}} \qquad \omega_{0_{3,4}} = \pm\sqrt{\frac{-\mathrm{frac}-\sqrt{\mathrm{frac}^2+4\frac{{\mathrm{R_{eq}}}^2}{\mathrm{den}}}}{2}} \tag{9}$$

$$den = {L_{\mathrm{s}}}^2 L_{\mathrm{p}} C_{\mathrm{p}} - M^2 L_{\mathrm{s}} C_{\mathrm{p}} \qquad frac = \frac{{R_{\mathrm{eq}}}^2 L_{\mathrm{p}} C_{\mathrm{p}} - {L_{\mathrm{s}}}^2}{den}. \tag{10}$$

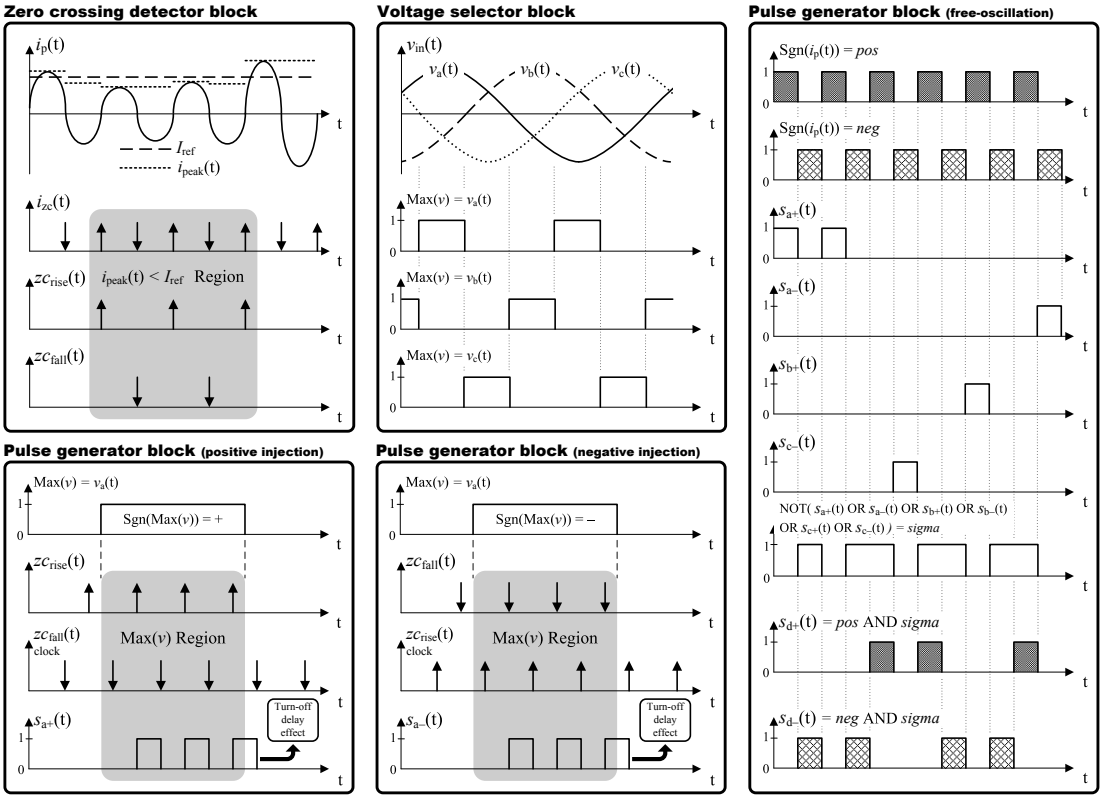

Figure 6: Block diagram operations.

During a no-load condition ($R_{\mathrm{L}} = \infty$), the last term in (7) can be ignored and the resonant equation is simplified to:

$$\omega_{0_{1,2}} = \pm \frac{1}{\sqrt{L_{\mathrm{p}} C_{\mathrm{p}}}}. \tag{11}$$

A positive, real and non-zero frequency is used to calculate capacitor and inductor voltages as well as the resonant current.

Primary current during a load condition

The load condition occurs when $R_{\mathrm{L}} \neq 0$. During a resonant period, the primary current can be represented as:

$$|\mathbf{i_p}| = \frac{V_{\mathrm{s}}({R_{\mathrm{eq}}}^2 + \omega_0^2 {L_{\mathrm{s}}}^2)}{\omega_0^2 M^2 R_{eq}}, \tag{12}$$

which can also be regarded as a maximum reference current that can be used in the controller.

Capacitor and inductor voltages

During a resonant period, the capacitor voltage can be calculated as:

$$|\mathbf{V_C}| = \frac{\mathbf{i_p}}{\omega_0 C_{\mathrm{p}}}, \tag{13}$$

while for the inductor voltage, the reactive part of the equation (6) needs to be incorporated in the calculation as given below:

$$|\mathbf{V_L}| = \mathbf{i_p} \left(\omega_0 L_{\mathrm{p}} - \frac{\omega_0^3 k^2 L_{\mathrm{p}} {L_{\mathrm{s}}}^2}{{R_{\mathrm{eq}}}^2 + \omega_0^2 {L_{\mathrm{s}}}^2} \right). \tag{14}$$

In a no-load condition, the equation for the inductor is reduced to:

$$|\mathbf{V_L}| = \mathbf{i_p} \omega_0 L_{\mathrm{p}}. \tag{15}$$

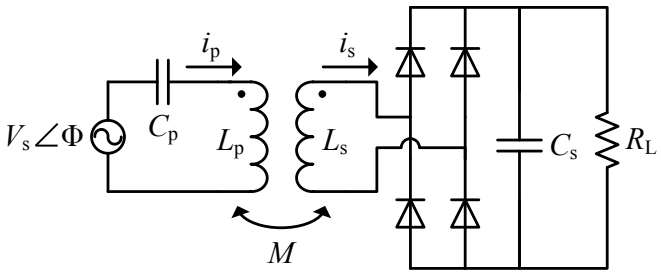

(a) An equivalent primary circuit with a secondary pick-up.

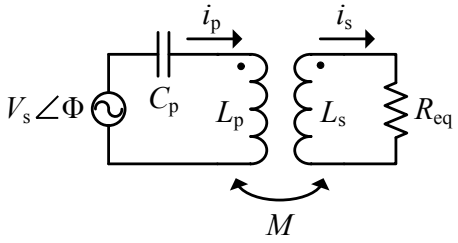

(b) A secondary circuit simplification.

Figure 7: Circuit simplifications.

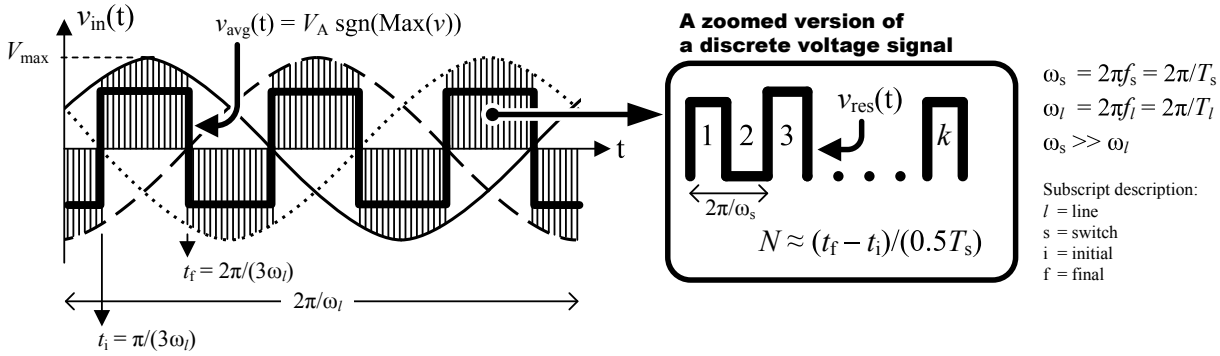

Figure 8: A resonant voltage averaging illustration.

Simulation Results

Converter operations during a closed-loop arrangement under ideal no-load and load conditions were simulated by PLECS. The simulation study only focused on some effects due to varying distance between the primary and secondary circuits which is represented by a coupling factor k. The value of $k = 0.9$ was chosen to represent a strong coupling while $k = 0.1$ characterizes a weak one. The value of each circuit element in Figure 7b for the simulation works is given in Table II. The capacitor and inductor values were chosen in a way that the circuit resonant frequency during $R_L = 20\ \Omega$ and $k = 0.9$ is close to 80 kHz. The current reference (I_{ref}) was kept constant during the whole simulations.

Table II: Circuit component values

	V_{rms}	ϕ	C_p	L_p	L_s	k	I_{ref}
Values	230 V	0°	40 nF	0.5 mH	0.5 mH	0.1, 0.9	20 A

No-load condition

In a no-load condition, R_L was set to infinity. For strong and weak coupling cases, the three-phase input, switching signals and the primary current are presented on the left side plots of Figure 9. On the other hand, primary capacitor and inductor voltages as well as an input current are shown on the right side of the same figure.

From the left plots of Figure 9, it can be seen that Sa+, Sd+ and Sd− are turned-on and off at the zero crossings of the primary current. This creates ZCS effect that reduces switching losses in the converter. Since there is no load connected and the circuit consists of ideal components, there is no power loss and the current is circulating indefinitely. The controller was able to detect the actual peak current well, therefore only five pulses of injection mode were produced in Sa+ plot. After the current reaches the reference point (20 A), the converter only switches Sd+ and Sd− to keep the current flowing. The peak value of the current is 25.471 A. In an uncontrolled mode, the current amplitude will grow indefinitely since the circuit is ideal. Equation (11) does not contain the k factor, therefore the resonant frequency during a no-load is independent of the coupling factor. This leads to the same capacitor and inductor voltages for strong and weak couplings. Using C_p and L_p values provided in Table II, the calculated resonant frequency for no load cases is 35.588 kHz.

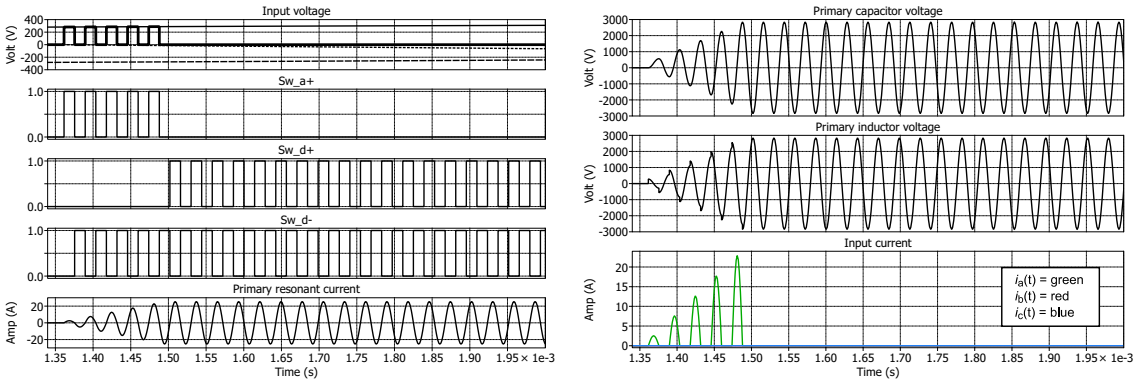

Figure 9: Simulation results for $k = 0.9$ and $k = 0.1$ under no load condition. The data was taken from $t = 1.34$ ms to $t = 2$ ms.

The right hand plots of Figure 9 show the voltage across the capacitor and inductor as well as input current due to switching actions during no load case. The voltage amplitude varies based on the coupling condition as described by voltage equations given in (13) and (15). The weak coupling makes the amplitude higher than the strong one. Using the current peak value, the resonant frequency and some values from Table II, both calculated capacitor and inductor peak voltages are equal to 2.848 kV.

In the current plot, $i_{\mathrm{a}}(\mathrm{t})$, $i_{\mathrm{b}}(\mathrm{t})$ and $i_{\mathrm{c}}(\mathrm{t})$ indicate input currents flowing from $v_{\mathrm{a}}(\mathrm{t})$, $v_{\mathrm{b}}(\mathrm{t})$ and $v_{\mathrm{c}}(\mathrm{t})$ respectively. Since the injection mode only occurs during $v_{\mathrm{a}}(\mathrm{t})$ at its positive cycle, the plot only shows $i_{\mathrm{a}}(\mathrm{t})$ during this period. Based on the input current plot, the switching actions create disturbances on the input line, therefore an Electromagnetic Interference (EMI) filter is needed to reduce the disturbance that can affect other electrical or electronic devices connected on the same power line. The design and analysis of the filter will be investigated after a practical converter is made and studied.

Load condition

The load R_{L} is chosen to be 20 Ω, and R_{eq} becomes 16.211 Ω. The same plot data as in a no-load condition section are presented in Figure 10 for $k = 0.9$, and Figure 11 for $k = 0.1$. A longer timescale than in no load case is used to show the input current behavior from each input phase.

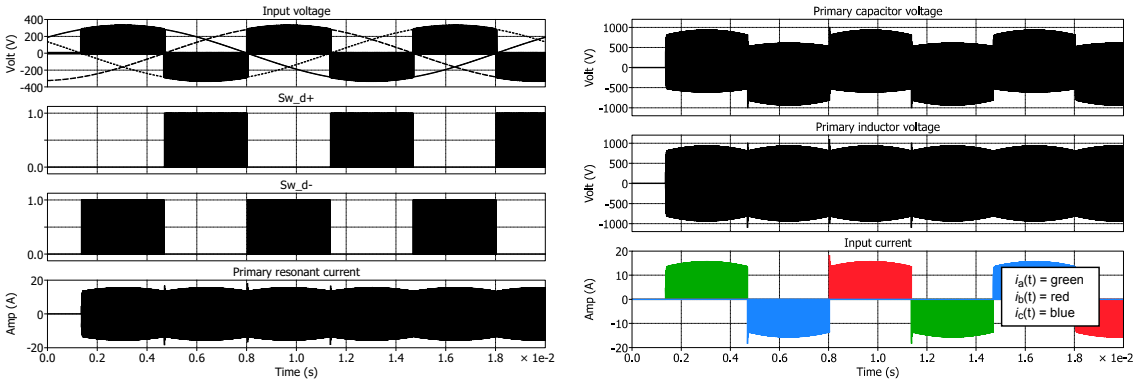

Figure 10: Simulation results for $k = 0.9$ and 20 Ω load condition. The data was taken from $t = 0$ ms to $t = 20$ ms.

The calculated resonant frequency for each case is 80.949 kHz for $k = 0.9$, and 35.764 kHz for $k = 0.1$. The frequency shift will not be a problem for the controller to adapt since driving pulses for all switches are constructed based on the resonant current. When the system is in a strong coupling condition, the steady-state primary current cannot reach the 20 A reference. In this case, the controller will keep injecting current indefinitely and all its switches will be utilized. During the positive input voltage cycle, Sd+ switch is not employed since a full cycle of the free-oscillation mode is never used. For the same reason, Sd− switch is not applied during the negative input voltage cycle. The maximum current amplitude can be calculated using equation (12) where V_{s} is obtained through equation (4). The calculated value of V_{s} and maximum current amplitude for the strong coupling case are 197.729 V and 15.119 A respectively.

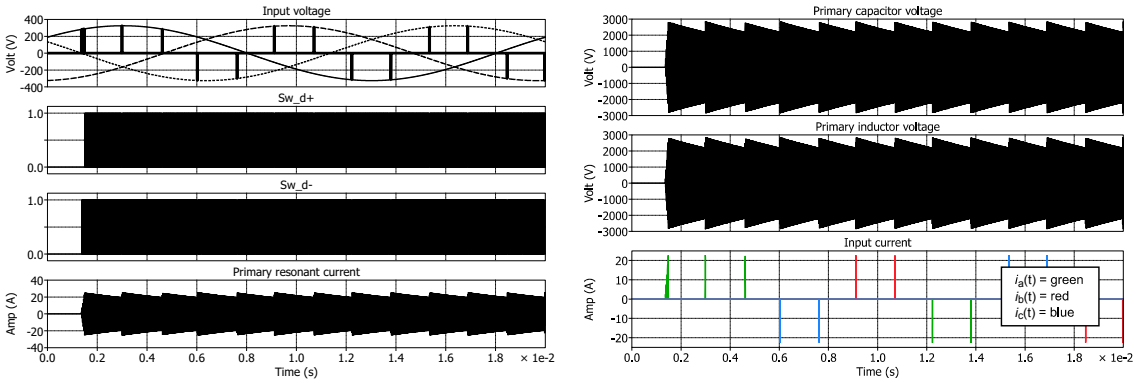

Figure 11: Simulation results for $k = 0.1$ and 20 Ω load condition. The data was taken from $t = 0$ ms to $t = 20$ ms.

In a weak coupling condition, the current can reach the reference point. The k factor in (12) is located in the denominator of the equation, therefore a smaller k, leads to a higher primary resonant current and vice versa. The calculated V_s and maximum current amplitude in this case are 197.773 V and 1.245 kA correspondingly, therefore the 20 A reference value can be reached.

Conclusion

A unique direct three-phase to single-phase AC/AC converter has been proposed in this paper. The converter operations are based on injection and free-oscillation of resonant current commutations. An on-off current controller general idea has been explained and it is used to control the converter's primary resonant current. The converter's behaviors at ideal no-load and load configurations have been presented using simulation data. Theoretical studies have been done to explain some of the behaviors in a steady-state manner. From simulation results, it can be seen that a coupling factor is proportional to a resonant frequency. The higher the coupling value, the higher the frequency and vice versa. Since zero coupling equals to a no-load condition, the frequency is the lowest in this case. In a practical implementation, the frequency can be used as an indicator that the load is detached. A real device of the proposed converter is currently being made, and more complete results of theoretical and experimental studies will be analyzed and reported in future publications.

References

[1] M.P. Kazmierkowski, A.J. Moradewicz, Unplugged but Connected: Review of Contactless Energy Transfer Systems, *IEEE Industrial Electronics Magazine*, vol. 6, issue 4, pp. 47-55, Dec 2012.

[2] Hao Leo Li, Hu, A.P., Covic, G.A., A Direct AC-AC Converter for Inductive Power-Transfer Systems, *IEEE Transactions on Power Electronics*, vol. 27, issue 2, pp. 661-668, Jun 2011.

[3] Nam, I., Dougal, R., Santi, E., Optimal design method to achieve both good robustness and efficiency in loosely-coupled wireless charging system employing series-parallel resonant tank with asymmetrical magnetic coupler, in *Proc. IEEE Energy Conversion Congress and Exposition* , Denver, USA, Sept 2013 , pp. 3266-3276.

[4] Hunter Hanzhuo Wu, Grant Covic, A Low Energy Storage IPT System using AC Processing Controllers, *Proc. IEEE Conference on Industrial Electronics and Applications*, Beijing, China, Jun 2011, pp. 351-356.

[5] Oghafi, V., Radan, A., Bidirectional switch commutation for high frequency UPF matrix converter supplying Inductive Power Transfer system, in *Proc. Power Electronics, Drive Systems and Technologies Conf.*, Tehran, Iran, Feb 2014 , pp. 422-427.

[6] Covic, G.A., Boys, J.T., Modern Trends in Inductive Power Transfer for Transportation Applications, *IEEE Journal of Emerging and Selected Topics in Power Electronics*, vol. 1, issue 1, pp. 28-41, May 2013.

[7] Robert L. Steigerwald, A Comparison of Half-Bridge Resonant Converter Topologies, *IEEE Transactions on Power Electronics*, vol. 3, issue 2, pp. 174-182, Apr 1988.